



Copyright Notice

© 2016 IEEE. Personal use of this material is permitted. Permission from IEEE must be obtained for all other uses, in any current or future media, including reprinting/republishing this material for advertising or promotional purposes, creating new collective works, for resale or redistribution to servers or lists, or reuse of any copyrighted component of this work in other works.

This document was downloaded from Chalmers Publication Library (<http://publications.lib.chalmers.se/>), where it is available in accordance with the IEEE PSPB Operations Manual, amended 20 Nov. 2015, Sec.

8.1.9 (<http://www.ieee.org/documents/opsmanual.pdf>)

(Article begins on next page)

Microwave-based stroke diagnosis making global pre-hospital thrombolytic treatment possible

Mikael Persson, Andreas Fhager, Hana Dobšiček Trefná, Yinan Yu, Tomas McKelvey,
Göran Pegenius, Jan-Erik Karlsson, Mikael Elam

Abstract—Here we present two different brain diagnostic devices based on microwave technology and the associated two first proof of principle measurements that show that the systems can differentiate hemorrhagic from ischemic stroke in acute stroke patients, as well differentiate hemorrhagic patients from healthy volunteers. The system was based on microwave scattering measurements with an antenna system worn on the head. Measurement data were analyzed with a machine-learning algorithm that is based on training using data from patients with a known condition. CT images were used as reference. The detection methodology was evaluated with the leave-one-out validation method combined with a Monte Carlo based bootstrap step. The clinical motivation for this project is that ischemic stroke patients may receive acute thrombolytic treatment at hospitals, dramatically reducing or abolishing symptoms. A microwave system is suitable for pre-hospital use, and therefore has the potential to allow significantly earlier diagnosis and treatment than today.

Index Terms—Microwave system, stroke diagnostics, subspace distance classification.

I. INTRODUCTION

THE global cost of stroke, including direct health care cost, direct non-medical cost and indirect cost, is hard to assess but the total 2010 European cost has been estimated to 64.1 billion € [1]. While the cost for society is huge, the human cost of stroke is horrific. Out of the sufferers of stroke, 5 million people/year die and another 5 million are permanently disabled [2]. The incidence of stroke in patients below 65 years of age is increasing and presently constitutes 20% of all strokes. Almost 80% of all strokes are ischemic (obstructed

blood flow), while the rest are hemorrhagic (bleeding into brain or on the surface of the brain). In the western world, stroke is placed third among reasons for acute death, and first among reasons for neurological dysfunction, resulting in most days of hospital nursing and therefore the most costly disease within western world health care [3]. Among stroke survivors, 20% have serious remaining dysfunctions. A much larger proportion has less conspicuous dysfunctions, which still seriously affect quality of life for the patient and relatives.

Early thrombolytic treatment of ischemic stroke is today an established procedure, [4]–[6], but could be disastrous if performed on a patient with a hemorrhagic stroke. Computer Tomography (CT) and sometimes Magnetic Resonance Imaging (MRI) are used to exclude hemorrhagic stroke. The sooner after onset of symptoms the thrombolytic therapy is initiated, the better the effect. According to European guidelines, treatment after 4.5h have elapsed since start of symptoms is not approved as the potential benefit does not outweigh the risk for hemorrhagic complications, which increases with time. While 20-30% of patients arriving at specialized stroke centers may receive thrombolytic treatment, [7], [8] only 1-8% of the entire stroke patient population are given such treatment, [9], mainly due to long lead times in transport to and from the diagnostic instruments, [10], [11]. Although solutions for CT scanning in ambulances have been presented, [12], the global scale of this clinical dilemma motivates efforts to develop new simplified diagnostic procedures capable of pre-hospital differentiation between ischemic and hemorrhagic stroke.

Several different technologies have been researched with the aim to develop a compact system that can be used to distinguish ischemic from hemorrhagic stroke in a pre-hospital setting. Ultrasonography can be used to identify large vessel occlusions in acute stroke care, [13] but cannot exclude hemorrhagic transformation of the resulting ischemic regions. Impedance tomography has been proposed as a possible technology to detect ICH in an animal model, [14] and impedance spectroscopy has been suggested as a method to detect stroke related brain asymmetries in man, [15]. While less developed in medical diagnostics, microwave propagation in human tissues has an advantage over both impedance and ultrasound via the easy penetration of the human skull. This is the fundamental basis for the present effort.

Microwave imaging techniques for biomedical applications have been researched for almost three decades. Due to the inherent scattering nature of propagating microwaves in inhomogeneous media, computationally very demanding algorithms are used. It is not until the latest 5-10 years that the

M. Persson, A. Fhager H. Dobšiček Trefná are with Signal Processing and Biomedical Engineering, Dept. of Signals and Systems, Chalmers University of Technology, Göteborg, Sweden, and MedTech West, Göteborg, Sweden.

T. McKelvey and Y. Yu are with Signal Processing and Biomedical Engineering, Dept. of Signals and Systems, Chalmers University of Technology.

G. Pegenius is with Inst of Neuroscience and Physiology, Dept. of Clinical Neurophysiology, Sahlgrenska Academy, Göteborg University, Sweden.

J.-E. Karlsson is with Neuro-division, Sahlgrenska University Hospital, Göteborg, Sweden

M. Elam is with Inst of Neuroscience and Physiology, Dept. of Clinical Neurophysiology, Sahlgrenska Academy, Göteborg University and Neuro-division, Sahlgrenska University Hospital and MedTech West, Göteborg, Sweden

This work was supported in part by VINNOVA (Swedish Government Agency for Innovation Systems) within the VINN Excellence Centre Chase, by SSF (Swedish Foundation for Strategic Research) within the Strategic Research Centre Charmant, and partly by the Swedish Research Council (grants no. 4627 and 12170).

Manuscript received January 28, 2014, revised April 22, 2014, and accepted May 16, 2014.

Copyright (c) 2013 IEEE. Personal use of this material is permitted. However, permission to use this material for any other purposes must be obtained from the IEEE by sending an email to pubs-permissions@ieee.org.

required computational power has become readily available and that clinically relevant results have been obtained. A large part of the efforts have been devoted to microwave imaging for breast cancer detection. Currently this application has come to a phase of initial clinical studies, [17]–[19] where encouraging results have been obtained.

The microwave technique is dependent on the existence of a dielectric contrast between different tissues. A number of studies of the dielectric properties of different human tissue have been made, [20]–[23] and there is a clear indication of a significant contrast between blood and white and gray brain matter. Originating in our own work with microwave tomography applied to breast cancer detection, [24], we have developed a helmet with microwave patch antennas, signal processing methods based on a machine learning algorithm and have performed numerical and phantom studies of hemorrhagic stroke detection, [25], [26], with encouraging results. This application is currently attracting increasing interest among researchers. Recently both numerical studies [27], [28] as well as a phantom study [29] show the ability to detect the presence and location of a bleeding stroke inside the skull. The ambition with our research project is to develop a system that can be used upon arrival in the emergency room, or by ambulance personnel at the scene of incident. The relative simplicity and size of a microwave-based diagnostic system underlined the possibility of creating an ambulance-based pre-hospital diagnostic system for stroke patients.

As already mentioned, a mobile CT-equipped stroke unit enabling pre-hospital diagnosis and treatment has been developed, and a recent trial showed that it achieved a marked reduction of latency from symptom-onset to thrombolytic treatment compared to previous interventional studies [9], [12]. Although CT-equipped vehicles constitute a formidable technical achievement, they may primarily be a solution for countries with a well organized and financed health care system, densely populated areas with well developed traffic and telecommunication infrastructure. Affordable and easily transported equipment for the diagnosis of stroke will remain a priority for countries not meeting this description. A microwave-based system has the advantage of being completely safe and without side effects. The method also has the potential of becoming quite cost effective as the component costs are driven down by the considerably larger telecom industry. Apart from pre-hospital diagnosis and treatment, another application of microwave-based stroke detection may be for monitoring patients undergoing thrombolytic therapy or patients hospitalized after a transitory ischemic attack.

In this paper we discuss the background, design and signal analysis of two microwave based stroke detection systems. We have also performed proof of concept testing using the two prototype systems on patients and healthy volunteers. In the first study we used a bicycle helmet, in which 10 patch antennas were mounted. Measurements were performed using a standard network analyzer and switch box. In the second study a custom-built helmet with 12 antennas was used. This time a dedicated and integrated network analyzer and switching solution were used.

II. MEASUREMENTS

A. Fundamental Principles for Measurements

Stroke diagnosis with a microwave system is based on measurements and analysis of signals that are transmitted through the brain. The antennas are distributed over the entire head to achieve high detection sensitivity. This is illustrated in Fig. 1. One at a time, each antenna is used as a transmitter,



Figure 1. The 3-d distribution of the isosceles triangle patch antennas

with the remaining antennas in receiving mode, Fig. 2 (a). In total a large number of transmission measurements are made. The basis for detection is to analyze the scattered wave pattern caused by the variations in dielectric contrast in healthy and normal tissue. The dielectric properties of white and gray brain matter at the frequency 1.0 GHz has been measured to $\epsilon_r = 38.6$, $\sigma = 0.62$ S/m and $\epsilon_r = 52.3$, $\sigma = 0.99$ S/m respectively, [20]–[23]. The corresponding properties for blood has been measured to $\epsilon_r = 61.1$, $\sigma = 1.58$ S/m. The fact that the properties of blood are different from white and gray matter also provides the basis for detecting the pool of blood caused by a hemorrhagic stroke. Also in the case of an ischemic stroke caused by a blood clot obstructing a vessel, there exists a basis for detection, Fig. 2 (b). The dielectric properties are strongly dependent on the circulation of blood and the oxygenation level. To our knowledge, no in vivo measurements have been made of the dielectric properties of a brain area influenced by reduced circulation. However, tests on bovine brain tissue have shown that dielectric parameters change as a function of time after death [30]. However, these measurements were made at a lower frequency range, 20kHz – 100MHz, than those used in these studies.

B. The Prototype Design Principle

In this section the design of the two systems are described. In order to provide a comfortable fit, patch antennas with a flat surface facing the skull were used. To accommodate varying skull size/shape of patients, containers of soft plastic were placed between skull and antennas and filled with water to fill the gap. The use of the plastic containers ensured a good electromagnetic coupling between the antennas and the skull. The measurements were made with a two-port network

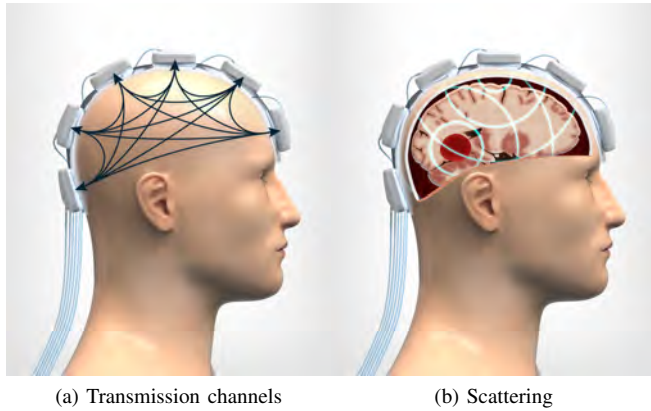


Figure 2. (a) The transmission channels measured between each antenna pair. (b) Scattered signal due to accumulated blood pool.

analyzer integrated with a switch matrix module and computer-controlled in order to automate the measurement procedure for all antenna pairs. The power was about 1 mW, transmitted from one antenna at the time. This is about 100 times lower than the maximum averaged output power of 125 mW that is transmitted from a GSM-cell phone. No adverse effects are therefore expected from use of the developed systems.

The patch antennas used in these two systems were the same as those used in the hyperthermia applicator developed at Chalmers [31]. This reference contains a detailed description of the antenna. In the second system the antennas were slightly modified with the connector placed on the side of the antenna rather than on the back. However the change of positions were made such that the antenna characteristics were unaltered. This type of antenna is more broadband than for example a monopole or a dipole. In the present helmet-design the antenna operates close to the skull, i.e. in the near-field. In addition to the antenna design the structures in close proximity of the antenna, e.g. plastic containers, skull, helmet, etc. are also influencing the antenna performance. The characterization of the individual antennas and the antenna array must therefore be made in realistic operating conditions, i.e. when it is worn. Under such conditions the reflection coefficients show a resonance frequency at 1.2–1.3 GHz. An individual variation can be seen between antennas, due to the reasons just mentioned. The reflection coefficient is typically below -10 dB in a 500 MHz band around the resonance frequency. To illustrate this, the reflection coefficients showing the typical response for three of the twelve antennas, in the second system, are plotted in Fig. 3. For the transmission coefficient, the maximum value is typically found, in the range 0.8–1.3 GHz. The reason for this lower frequency range is that conductivity of brain tissue increases with frequency, and that the propagation distance between different antenna combinations vary. These two parameters, distance and conductivity, together determine at which frequency the maximum transmission is obtained. The resulting maximum transmission coefficient is typically in the range -20 – -40 dB. Transmission coefficients above -40 dB are typically found in a band 1.0 – 1.5 GHz around this maximum, and this is where we expect to obtain the

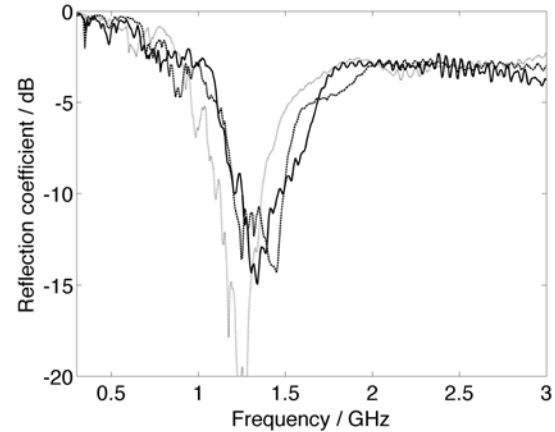


Figure 3. Examples of reflection coefficients for three different antennas on the helmet. The remaining antennas show similar characteristics.

best diagnostic performance for our system. In this frequency range signals propagating through the thickest part of the head are above the noise floor of the microwave measurement units, and can thus reliably be detected by all antenna pairs. In the present studies, every channel was measured over a large band of frequencies, 0.3–3.0 GHz, which is more than we expect to be useful. Also the transmission coefficients are affected by the same variability due to near field effects as are the reflection coefficients. To exemplify, transmission coefficients for neighboring antennas, i.e. the pair with the highest transmission, and the diagonally opposing antennas, i.e. the antennas with the lowest transmission, have been plotted in Fig. 4.

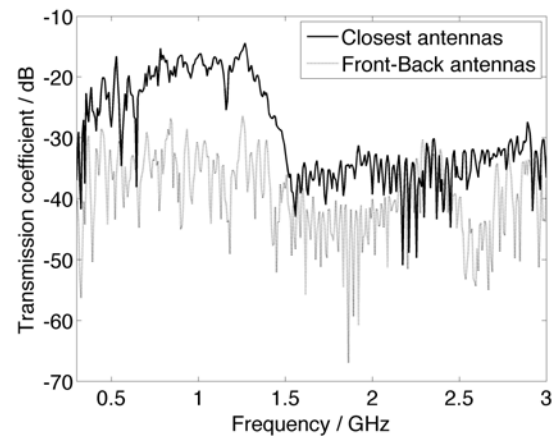


Figure 4. Examples of transmission coefficients between the antenna on the front and the back of the skull, and between the antennas on the front and its closest neighbor.

At the lower end of the measured frequency band a large variability is seen in the measurements, even between measurements on the same patient. This can be understood in terms of capacitive coupling between the antennas, cables and the surroundings, and makes the measurements less reliable, since they are influenced by sources originating from outside the

skull. At the upper end of the frequency scale disturbances can also be anticipated, both in terms of reduced signal strength caused by the increasing losses in the tissue, but also due to variability introduced by the decreased wavelength. When wearing the helmet there will be individual variations in the fitting due to the physique of the patient, e.g. skull size, amount of hair, amount of water in the water containers, and positioning of the helmet, etc. In terms of wavelengths, these variations increase with frequency and cause corresponding uncertainty in the data.

The signal analysis aims at extracting useful information with respect to the optimal antenna performance range and to remove the effect of errors. It is however difficult to exactly determine the limits where the data is useful or not. The approach in these studies has been to consider the useful frequency interval as unknown and as a parameter to be determined in the development procedure and in the clinical testing.

C. Technical development in preparation for clinical tests

In the development towards a microwave based stroke diagnostics device the first step was to design an antenna system that could be fitted on the head and used for microwave scattering measurements. This was performed as a numerical study in the simulation software CST [25]. The simulation was based on a head model from the Visible Human Project [32] male data set. In this model a spherical volume of blood was placed in order to simulate a hemorrhagic stroke [25]. The bleeding was centered 45 mm below the skin surface and positioned just below one antenna. Bleedings ranging 5-30 mm in radius were used for the simulations. When comparing the signal with that of a normal brain a detectable variation in the range 0.5-3 dB in the signal amplitude was found. This is within practically measurable limits and an encouraging result. The results are similar when the bleeding is placed between two antennas, but instead using transmission data for the detection.

A prototype system was then designed and built. It consisted of antennas sending and receiving microwave signals, mounted in a helmet. The helmet is shown in Fig. 5. In this prototype, ten antennas were used, and they are here visible because plastic containers for the matching liquid have been partly removed. In the right part of the helmet, it can however still be seen. This is the same helmet that was used in the first patient study.

In this system a total of 45 independent transmit-receive channels were measured. A single frequency measurement gives the scattering parameter, and measurements were performed over a large number of frequencies. The microwave measurement device was a fully computer-controlled system built on a two-port network analyzer (Agilent E8362 B PNA) as the transmit/receive unit. To fully automatize the experiment, a 2:32 switch multiplexer module (Cytec CXM/128-S-W) was used. The channel isolation was 120 dB.

As a next step this system was used in a lab test using tissue realistic phantom material. The helmet shown in Fig. 5 was used for these measurements. The aim was to model bleedings

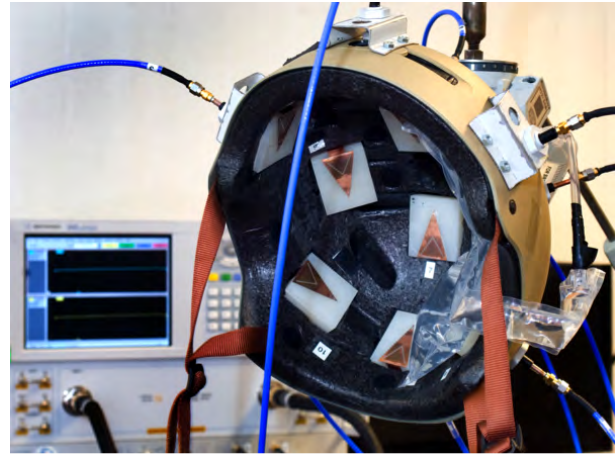


Figure 5. The first prototype system, in which the ten antennas have been mounted on a bicycle helmet. To the right, in the helmet, plastic bags used for the matching liquid can be seen.

of different sizes, and to measure and classify these bleedings. By mixing sugar, salt, water and agar a brain phantom with the same dielectric properties as gray matter was created, Fig. 6 (a). Using the same ingredients, with different relative ratios, phantom material with the same properties as blood was also created. Measurements were made on the brain phantom, before and after insertion of blood phantoms of volumes 1, 3, 5 and 10 ml. The measurement data was analyzed with a subspace distance measure and has been reported in [33]. The results of the analysis are shown in Fig. 6 (b). Two main features of importance to our detection problem are worth noting. First, the subspace distances of all cases with a bleeding included are separated from the non-bleeding case. Second, the subspace distance is increasing monotonically with bleeding size. The error-bars show the variation in the leave one out validation.

During the lab tests and also the first patient study it became clear that the first prototype was not optimally designed for its purpose. The main problem was the mechanical strength of the structures holding the antennas in place were too weak. For the second patient study a more robust custom built helmet structure with 12 antennas was constructed, see Fig. 7. This gave 66 independent transmit-receive channels and a custom built and integrated network analyzer and switching solution were used. Specifications of the network analyzer was similar to the previous system, however signal isolation in the switch was 80 dB.

III. SIGNAL ANALYSIS

The microwave measurement data, in terms of the scattering parameters of the transmission channels, were then used in a hemorrhagic stroke detecting algorithm. The algorithm was trained using measurements from subjects with known conditions, i.e. supervised learning. Data from each channel are pre-processed by scaling the values such that the total signal power is equal for all channels. The complex values from all channels are organized into a single complex vector. Finally, the data is transformed by employing the logarithm

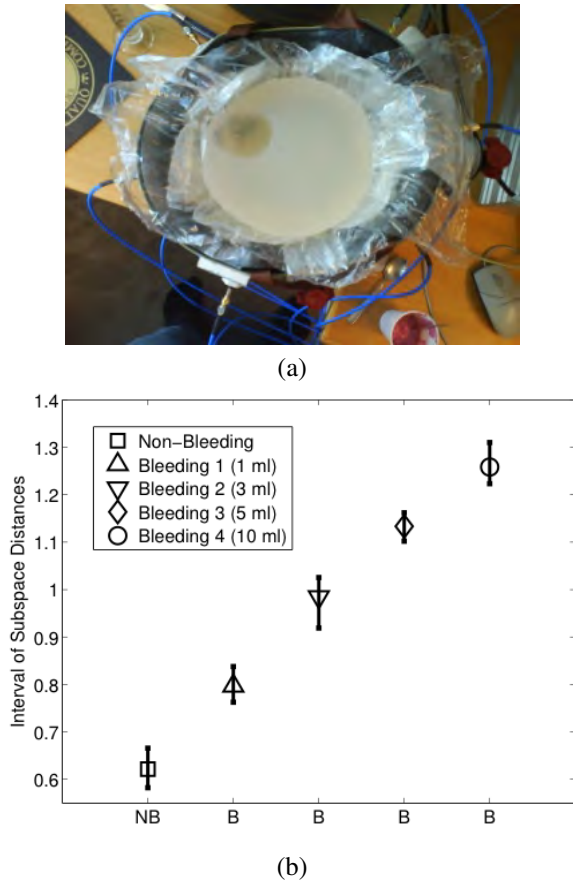


Figure 6. (a) The brain / blood phantom. (b) The subspace distance plotted for four different bleeding phantoms.

to each element of the data vector in order to bring the data to a better numerical range. The algorithm is based on the assumption that the noise free data vector from subjects with a hemorrhagic stroke belongs to a linear subspace and that the corresponding data from subjects with ischemic stroke belong to another linear subspace. Labeled training data is used to identify bases for these subspaces. In addition, since data from both classes share many common features, reduced size subspaces for each class are formed. This is accomplished by removing some of the directions in the subspaces that have the smallest angles between them. The principle of detection in the algorithm is based on projecting the data sample under test onto the two reduced subspaces and calculating the Euclidean distance of the projected data sample. The largest distance determines which class is selected, i.e. if a hemorrhagic stroke is detected or not. A decision offset can be introduced to change the performance of the detector and thereby improve the probability of detection, at the cost of an increased false alarm rate. The detection algorithm is a development of the original idea of a subspace classifier, i.e. CLAFIC, see [16]. So called matched subspace detectors, [34] are also based on similar ideas. In Section III-A information on measurement data, its structure and the data pre-processing applied are described. A thorough description of the classification algorithm is presented in Section III-B and the method of validation is



Figure 7. The second prototype system, in which the 12 patch antennas have been mounted on a custom built supporting structure.

detailed in Section III-C.

A. Measurement data and pre-processing

The raw measurement data provided by the antenna array system are samples of the complex scattering matrix for a given set of frequencies. For a fixed frequency ω_k , the scattering matrix element with row index i and column index j describe the complex gain $s_{ij}(\omega)$ between the transmission antenna j and the receiving antenna i . For reciprocal systems the scattering matrix is symmetric $s_{ij}(\omega) = s_{ji}(\omega)$. Hence, for a reciprocal antenna system with n_a ports the scattering matrix has, at most, $d = \frac{n_a^2 + n_a}{2}$ unique values.

Each matrix element is normalized across the frequency dimension to equalize the power between channels. The magnitude of the scattering parameters have a large dynamic range. To mitigate this effect all normalized scattering values are transformed using the complex logarithm function. Finally all values from one measurement is embedded into a single complex vector $\mathbf{x} \in \mathbb{C}^d$. Hence, the elements of the data vector \mathbf{x} are the elements of the set

$$\{\log(s_{ij}(\omega_k)/c_{ij}) | k = 1, \dots, n_\omega, 1 \leq i \leq j \leq n_a\} \quad (1)$$

where n_ω is the number of measured frequencies and

$$c_{ij} = \sqrt{\frac{1}{n_\omega} \sum_{k=1}^{n_\omega} |s_{ij}(\omega_k)|^2} \quad (2)$$

is the normalization constant.

B. Supervised learning and classification

A detection or classification algorithm is a function which map the data vector $\mathbf{x} \in \mathbb{C}^d$ into a discrete variable c called a class label.

$$c = f(\mathbf{x}) \quad (3)$$

Here we consider the binary classification problem and hence c is binary, ie $c \in \{+, -\}$, a class of positives and a class of negatives. If a (statistical) model exists describing the underlying mechanism of how samples \mathbf{x} and the corresponding class label are connected, the function f can be derived in various ways [37]. In supervised learning the function f is inferred by selecting f from a class of functions based on a set of available labeled training samples $\{(c_i, \mathbf{x}^i)\}$. The stroke detection algorithm is based on a supervised learning method.

Here the set of classification functions is implicitly defined by an assumed model of the data. We assume data samples \mathbf{x} corresponding to class c are generated according to

$$\mathbf{x} = \sum_{k=1}^{m_c} \mathbf{u}_{c,k}^0 \alpha_k + \mathbf{e} = \mathbf{U}_c^0 \boldsymbol{\alpha} + \mathbf{e} \quad (4)$$

where \mathbf{U}_c^0 is a matrix containing the basis vectors $\mathbf{u}_{c,k}^0$ as its columns and $\boldsymbol{\alpha}$ represents the corresponding basis weight vector for the specific sample \mathbf{x} . The vector \mathbf{e} is the error between the model $\sum_{k=1}^{m_c} \mathbf{u}_{c,k}^0 \alpha_k$ and the measurement \mathbf{x} . The integer m_c is the dimension of \mathbf{U}_c^0 and we assume it is significantly smaller than the data dimension, ie $m_c \ll d$.

Estimates of the bases are determined using training data for each class respectively. All training data samples for one class is assembled into a matrix

$$\mathbf{X}_c = [\mathbf{x}_c^1, \mathbf{x}_c^2, \dots, \mathbf{x}_c^{t_c}] \quad (5)$$

where \mathbf{x}_c^i denote sample i with label c and t_c denote the number of training samples with label c . Let the Singular value decomposition (SVD) [38] be given by

$$\mathbf{X}_c = [\mathbf{U}_c \quad \mathbf{U}_c^\perp] \begin{bmatrix} \boldsymbol{\Sigma}_c & 0 \\ 0 & \boldsymbol{\Sigma}_c^\perp \end{bmatrix} [\mathbf{V}_c \quad \mathbf{V}_c^\perp]^H \quad (6)$$

where $\boldsymbol{\Sigma}_c$ contains the m_c largest singular values of \mathbf{X}_c . The matrix $\mathbf{U}_c \in \mathbb{C}^{d \times m_c}$ is an estimate of the basis of class c . If the SNR is high, or if $m_c \ll t_c$ the range space of \mathbf{U}_c will be approximately the same as the range space of \mathbf{U}_c^0 in Eq. 4.

Since the bases of the two classes are derived from samples of data which are noisy the estimated bases will be perturbed. Signal directions in the two signal subspaces which are nearly co-linear will particularly lead to a high variability of the outcome of the classifier. Hence, dimensions in the two signal spaces which are nearly co-linear are removed. Proximity between subspaces are measured using the principal angles.

Definition 1 (Principal angles). [38]

The principal angles $0 \leq \theta_1 \leq \dots \leq \theta_m \leq \pi/2$ between the subspaces spanned by $\mathbf{U}_+ \in \mathbb{C}^{d \times m_+}$ and $\mathbf{U}_- \in \mathbb{C}^{d \times m_-}$ are defined as:

$$\cos(\theta_k) = \max_{\mathbf{q} \in \mathbf{U}_+, \mathbf{r} \in \mathbf{U}_-} \mathbf{q}^T \mathbf{r} = \mathbf{q}_k^T \mathbf{r}_k$$

subject to:

$$\|\mathbf{q}\| = \|\mathbf{r}\| = 1 \quad (7)$$

$$\mathbf{q}_i^T \mathbf{q}_i = 0, \quad \mathbf{r}_i^T \mathbf{r}_i = 0, \quad i = 1, \dots, k-1$$

where \mathbf{q}_i and \mathbf{r}_i are the principal vectors and $m = \min(m_+, m_-)$.

The vectors \mathbf{q}_1 and \mathbf{r}_1 defined by (7) are hence the vectors

from the two spaces spanned by \mathbf{U}_+ and \mathbf{U}_- respectively which have the smallest angle between them. Assuming, $m_+ = m_-$ and $\mathbf{U}_+^H \mathbf{U}_+ = \mathbf{U}_-^H \mathbf{U}_- = \mathbf{I}$, the SVD decomposition of the matrix product $\mathbf{U}_+^H \mathbf{U}_-$ readily yields a solution to the principal angle problem.

$$\mathbf{U}_+^H \mathbf{U}_- = \mathbf{Y} \text{diag}(\cos \theta_1, \dots, \cos \theta_m) \mathbf{Z}^H \quad (8)$$

Here

$$\mathbf{Y} = [\mathbf{y}_1 \quad \mathbf{y}_2 \quad \dots \quad \mathbf{y}_m] \\ \mathbf{Z} = [\mathbf{z}_1 \quad \mathbf{z}_2 \quad \dots \quad \mathbf{z}_m] \quad (9)$$

are unitary matrices and $\text{diag}(\cos \theta_1, \dots, \cos \theta_m)$ is a diagonal matrix with the non-negative singular values on the diagonal and

$$1 \geq \cos \theta_1 \geq \dots \geq \cos \theta_m \geq 0.$$

Reduced bases with the r closest directions removed are given by

$$\mathbf{U}_{r+} = \mathbf{U}_+ [\mathbf{y}_{r+1} \quad \dots \quad \mathbf{y}_m] \\ \mathbf{U}_{r-} = \mathbf{U}_- [\mathbf{z}_{r+1} \quad \dots \quad \mathbf{z}_m]. \quad (10)$$

The discrimination rule is defined by

$$f(\mathbf{x}) = \begin{cases} + & \text{when } \delta(\mathbf{x}) + \beta > 0 \\ - & \text{when } \delta(\mathbf{x}) + \beta \leq 0 \end{cases} \quad (11)$$

where

$$\delta(\mathbf{x}) = \|\mathbf{U}_{r+} \mathbf{U}_{r+}^H \mathbf{x}\|^2 - \|\mathbf{U}_{r-} \mathbf{U}_{r-}^H \mathbf{x}\|^2 \\ = \mathbf{x}^H (\mathbf{U}_{r+} \mathbf{U}_{r+}^H - \mathbf{U}_{r-} \mathbf{U}_{r-}^H) \mathbf{x} \quad (12)$$

The second equality in Eq. 12 follows since

$$\mathbf{U}_{r+}^H \mathbf{U}_{r+} = \mathbf{U}_{r-}^H \mathbf{U}_{r-} = \mathbf{I}.$$

The rule can be interpreted as follows. The data vector \mathbf{x} is projected onto the subspaces spanned by the matrices \mathbf{U}_{r+} and \mathbf{U}_{r-} respectively. The label is selected according to which of the projected vectors have the largest Euclidean length. A non-zero value of the decision offset β in Eq. 11 can be used to bias the detection towards class + if $\beta > 0$ and towards class - if $\beta < 0$. In comparison with [16], [34] the step where the nearly co-linear subspaces are removed is here added. This methodology was introduced in [35], [36].

In the stroke detection application three consecutive measurements are performed on each subject yielding the measurement set $\{\mathbf{x}^i | i = 1, 2, 3\}$. In order to reduce the variance of the classification result, a modified discrimination rule according to

$$f(\{\mathbf{x}^i\}_{i=1}^3) = \begin{cases} + & \text{when } \delta(\{\mathbf{x}^i\}_{i=1}^3) + \beta > 0 \\ - & \text{when } \delta(\{\mathbf{x}^i\}_{i=1}^3) + \beta \leq 0 \end{cases} \quad (13)$$

is employed where

$$\delta(\{\mathbf{x}^i\}_{i=1}^3) = \frac{1}{3} \sum_{i=1}^3 \|\mathbf{U}_{r+} \mathbf{U}_{r+}^H \mathbf{x}^i\|^2 - \|\mathbf{U}_{r-} \mathbf{U}_{r-}^H \mathbf{x}^i\|^2 \\ = \frac{1}{3} \sum_{i=1}^3 \mathbf{x}^{iH} (\mathbf{U}_{r+} \mathbf{U}_{r+}^H - \mathbf{U}_{r-} \mathbf{U}_{r-}^H) \mathbf{x}^i \quad (14)$$

which in effect uses the average of the three subspace distances

as the input to the threshold function in Eq. 13.

C. Performance assessment by cross-validation

The performance of the classification algorithm is measured by calculating the empirical *sensitivity* and *specificity* using leave-one-out (LOO) cross-validation. In standard LOO cross-validation, one sample is removed from the training data set and saved for testing the derived classifier. This procedure is repeated for all data samples and finally the empirical performance rates are calculated. The method gives unbiased performance estimates but has a high variance [37]. In this application three measurements from each subject are at hand. A straightforward use of the LOO approach, treating the three measurements as independent samples, would bias the result towards an overoptimistic performance. Hence, a modified LOO validation is employed, where all three data samples from one subject are removed when forming the training set. To reduce the variance of the performance estimate, a Monte Carlo based bootstrap method [39] is used where, in each LOO step, a sequence of training data sets are formed by randomly selecting one measurement out of the three for each of the subject, excluding the LOO subject. For each training data-set the classification function $f(\cdot)$ is constructed and the data from the subject left out is tested. The average performance is then estimated as the empirical outcome over all the randomly created training sets. In this application 100 random training-sets are used.

As the classification function is parametrized by the decision offset β in Eq. 13, the empirical estimates of the performance measures are a function of this offset. A receiver operator characteristic (ROC) curve is a visualization of how the *sensitivity* and *specificity* are related by plotting them against each other [40]. The result is a curve (parametrized by the offset β) which starts at coordinate (0,1) and ends at (1,0). The area under this curve (AUC) is a measure of the quality of the detector. An area of 1 corresponds to the case when the detector perfectly can separate the two classes and area of 0.5 correspond to a detector which randomly assigns the class label, e.g. coin-tossing.

IV. CLINICAL TESTING

We have made two consecutive explorative proof of principle studies, with the two different prototypes, performed at different hospital departments at Sahlgrenska University Hospital. While aiming for a microwave-based investigation as early upon onset of the stroke as possible, the experimental nature of the study did not allow a delay of routine clinical procedures. Only patients with clinically and/or radiologically established Intra Cerebral Hemorrhage (ICH) or Ischemic Stroke (IS), without a history of previous cerebrovascular events, were included in the studies. In each investigation, three consecutive microwave measurements were performed. Patient safety follow up was performed one day after the microwave-based investigation. Written, informed consent was obtained from each patient, before any study related procedure was initiated. The studies were approved by the local Ethical Review Board, and conducted according to Good Clinical Practice and the revised Declaration of Helsinki.

A. The first clinical study

The first study was performed at the department of clinical neurophysiology by engineering and neurophysiology staff. Here we summarize the main results from this study, performed with the same device used for our phantom studies (cf above, Fig. 5). The device was used to investigate 20 patients, diagnosed with acute stroke. The patients were studied in a time window of 7-132 hours after stroke onset, defined as last awareness of healthy condition. Out of the 20 patients enrolled, 9 patients were suffering from ICH and 11 patients from IS. Table I in the Appendix provides more detailed data about the patients. Scattering measurements in the frequency range from 885-1670 MHz were used in this study. Given the limited number of patients in the study, the LOO Monte Carlo approach described in Section III-C was used to assess the performance of the algorithm on these data.

The resulting Receiver Operating Characteristic (ROC) curve is shown in Fig. 8. The area under the curve (AUC) is 0.88 gives an indication of the strength of the detection algorithm. This result is obtained by removing 4 nearly co-linear dimensions resulting in a final subspace dimension of 4. Finally, the scatterplot in Fig. 9 shows the averaged squared subspace distance difference for each patient based on a leave-one-out validation method: The patients are arranged along the x-axis according to the time between stroke onset and the measurement occasion. With the hemorrhagic detector aimed at identifying all 9 patients with an ICH, 7 out of 11 IS patients were separated from the ICH group whereas 4 were not.

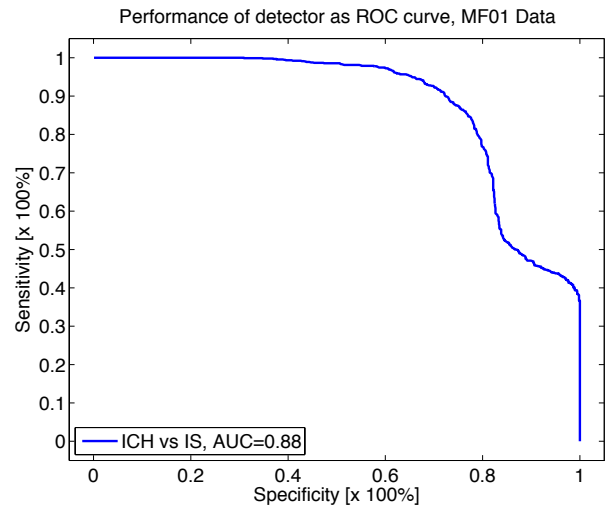


Figure 8. Summary of detector performance illustrated as an empirical ROC curve for ICH vs IS patients. The empirical performance is based on data from MF01 study and is obtained using a LOO Monte Carlo method. The ROC curves are parametrized by the decision offset β in (11). The area under the ROC curve (AUC) is 0.88.

B. The second clinical study

The second study was performed bedside within a neurology ward, by nursing staff. The patients were studied in a time window of 4-27 hours after stroke onset, defined as last awareness of healthy condition. The performance

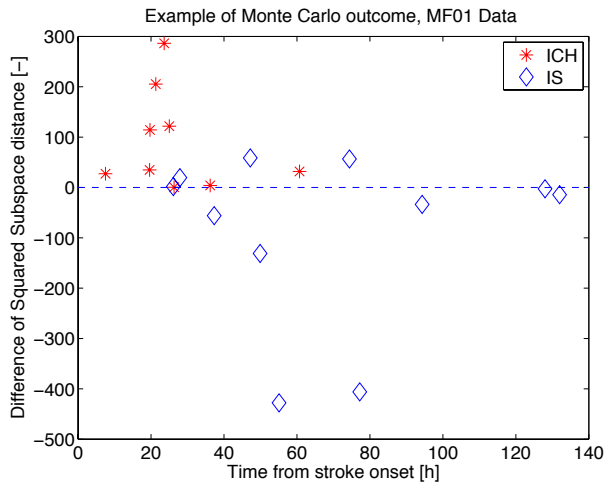


Figure 9. Illustration of the distribution of the decision variable, the difference between the squared subspaces distances evaluated for all patients in a leave-one-out validation. The x-axis corresponds to elapsed time from onset of stroke to time of measurement. Data is from ICH vs IS in first clinical study.

of the microwave measurement system with the associated algorithm was evaluated on the clinical data generated by measurements on 25 hospitalized stroke patients. Out of the 25 patients enrolled, 10 patients were suffering from ICH and 15 patients from IS, see Table II in the Appendix for more detailed information. The nurses performing the microwave-based assessment were blinded regarding the result of clinical and radiological investigations performed at admission. In addition, a group of healthy control subjects ($n=65$, 36 male, age range 23-74), recruited via advertisements within the hospital and university, were investigated.

The available data was grouped into two classes. In each case all measurements from patients with a bleeding stroke formed one class (ICH 10 subjects). The second class was formed in one of the following two ways:

- 1) Data from patients with an ischemic stroke (IS 15 subjects)
- 2) Data from healthy subjects (healthy 65 subjects)

We will refer to these test cases as 1) ICH vs IS, 2) ICH vs healthy. In each of the cases the objective of the detection is to discriminate ICH subjects from the others. The measurement bandwidth utilized was 857-1493 MHz and in the classification algorithm we remove 5 nearly co-linear dimensions resulting in a final subspace dimension of 4. The results from the detection of ICH patients, expressed as empirical probabilities from the Monte Carlo investigations are summarized in Figures 10-12. The resulting Receiver Operating Characteristic (ROC) curves are shown in Figure 10 where the upper graph illustrates the ICH vs IS case and the lower graph the ICH vs healthy case. The ICH vs IS case gave an AUC of 0.85, and ICH vs healthy case resulted in an AUC of 0.87. Note that the performance is increased when more subjects are included in the training data as compared to the base-line ICH vs IS case. Best performance is obtained when we discriminate ICH patients from healthy volunteers. In Figure 11 it is illustrated how different values of the decision offset β influence the

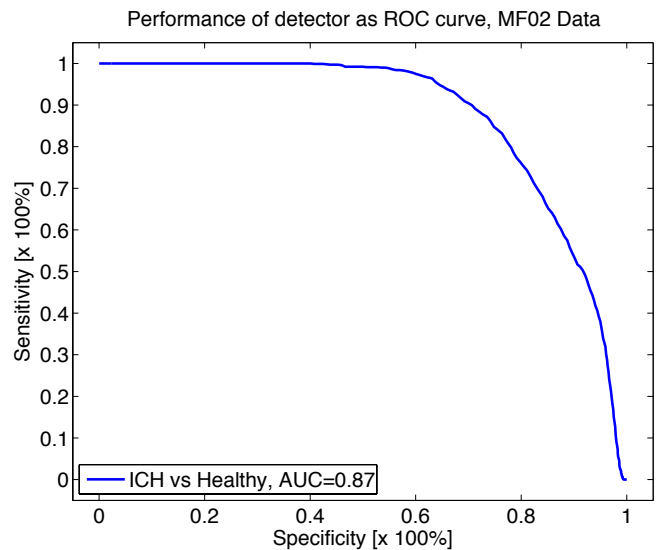
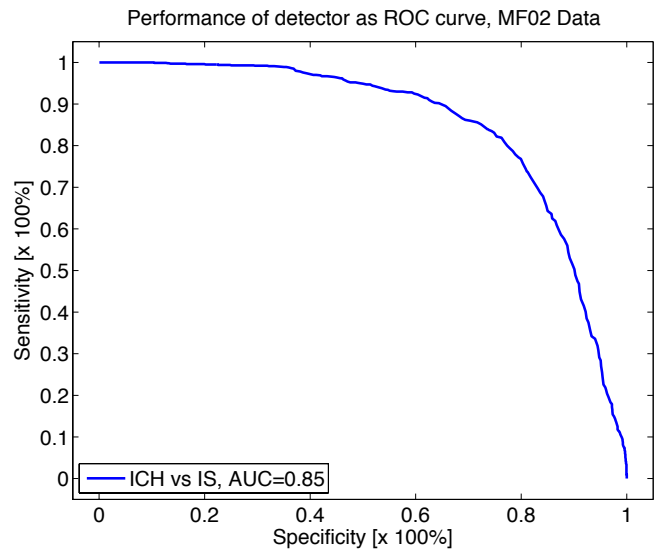


Figure 10. Summary of detector performance illustrated as empirical ROC curves for ICH vs IS patients (upper graph) and ICH vs Healthy group (lower graph). The empirical performance is based on data from MF02 Study and is obtained using the Monte Carlo method. The ROC curves are parametrized by the decision offset β in (11). The area under the ROC curve (AUC) is indicated in the legend of the plot for each graph.

sensitivity and specificity. The upper graph is for the ICH vs IS case and the lower graph is for the ICH vs healthy case. Finally, Figure 12 depicts a scatter plot from test case 1, ICH vs IS, illustrating the averaged squared subspace distance difference for each patient, based on the leave-one-out validation method. The patients are arranged along the x-axis according to the time elapsed between stroke onset and measurement. With the hemorrhagic detector aimed at identifying all 10 patients with an ICH, 14 out of 15 IS patients were clearly separated from the ICH group whereas 1 was not. As shown in Figure 12, the variability of the results is increased for patients measured 10h after stroke onset.

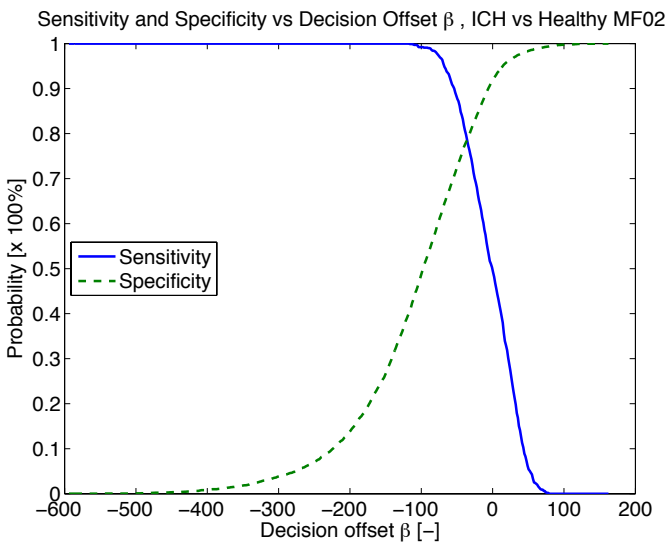
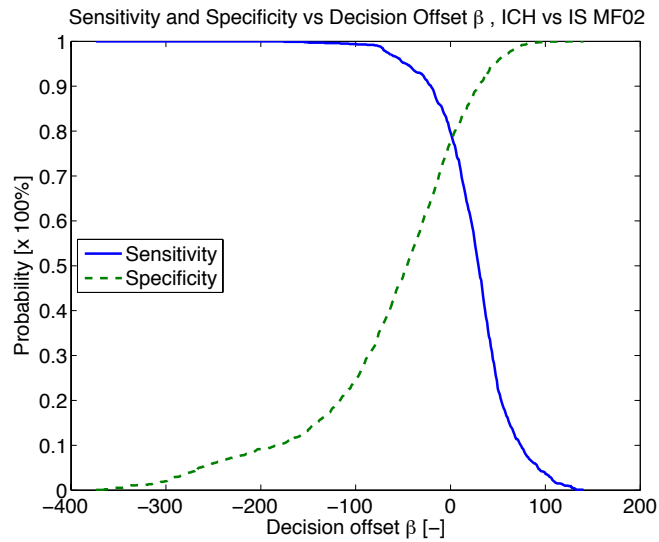


Figure 11. Summary of detector performance illustrated as how the Sensitivity and Specificity varies with the decision offset β in (11), for ICH vs IS patients (upper graph) and ICH vs Healthy group (lower graph). The empirical performance is based on data from MF02 Study and is obtained using a Monte Carlo method.

V. DISCUSSION

We have designed and built microwave-based measurement systems that can differentiate ICH from IS in acute stroke patients and ICH patients from healthy volunteers. Results from two different clinical pilot-studies demonstrate the effectiveness and limitations of the method developed. The finding, that our first- and second-generation systems generated similar stroke detection results is interesting as the two studies were made with completely different prototypes, performed at two separate departments at the hospital. Our continued clinical studies will evaluate improved analysis paradigms, as well as non-rigid caps carrying the antennas, with the ultimate aim to introduce a simple and affordable pre-hospital stroke diagnostic procedure.

The classification algorithms used for these two studies

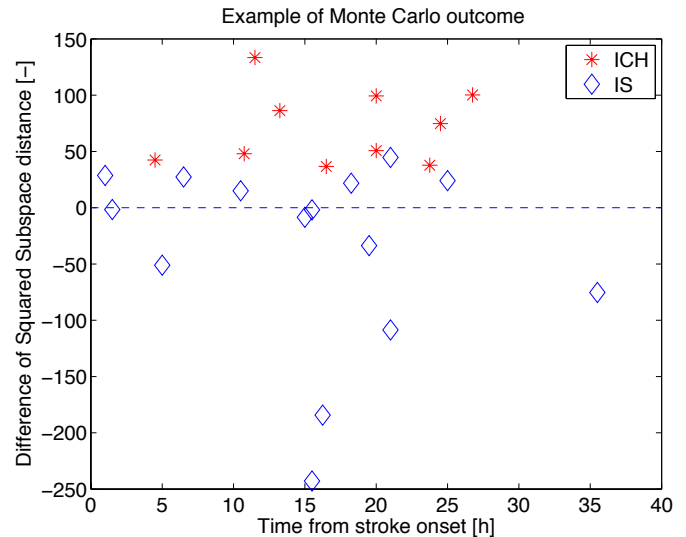


Figure 12. Illustration of the distribution of the decision variable, the difference between the squared subspaces distances evaluated for all patients in a leave-one-out validation. The x-axis corresponds to elapsed time from onset of stroke to time of measurement. Data is from case 1 ICH vs IS in MF02 study.

were derived using labeled sets of training data. The results in Figure 10 show an increased performance when healthy patients are used for training. That the comparison of ICH vs 65 healthy controls gave a better performance than the comparison ICH vs 15 IS was an expected finding, in all probability due to IS related brain edema increasing with the latency from IS onset. At 99.9% sensitivity to detect ICH, the proportion of IS patients safely differentiated was approximately 30%, whereas at 90% ICH sensitivity 65% of IS patients could be differentiated. A larger data-set resulting from an ongoing clinical study involving several hospitals in Sweden, aiming for as early investigation as possible, is expected to increase the predictive power of the algorithms, i.e. the capacity for ICH vs IS differentiation. However, even without such an improvement, the differentiating capacity reported here is of considerable clinical interest given the low percentage of ischemic stroke patients presently being diagnosed in time to get thrombolytic treatment (cf introduction). In a recent Swedish trial, a higher priority level given to stroke patients by the pre-hospital emergency medical service reduced time to arrival at a stroke unit and increased the percentage of patients receiving thrombolytic treatment from 10 to 24%, [41]. Adding reasonably safe pre-hospital information about type of stroke may be expected to improve these figures further, as well as the pre-hospital treatment and triage, [9].

Needless to say, an introduction of pre-hospital thrombolytic treatment based on a microwave scan diagnosis will have to await studies of larger clinical cohorts, and a full clinical translation can only be achieved when stroke clinicians in a non-blinded bedside situation can compare data provided by microwave-based classification to clinical status and other diagnostic procedures. Furthermore, we have presented the measurement system as a stroke detector and illustrated the

performance in terms of sensitivity and specificity measures in order to illustrate the merits of the system. However, the detector is based on comparing two derived measures, i.e. the sizes of the measured signal projected onto the subspaces representing each class. In a clinical setting we believe the physician will directly use these continuous measures in order to complement other diagnostic sources before making a final diagnosis.

VI. CONCLUSION

For the first time proof of principle have been presented that microwave-based measurements can differentiate ICH from IS in acute stroke patients as well differentiate ICH from healthy volunteers. The relative simplicity and size of microwave-based systems compared to CT or MR scanners make them easily applicable in a pre-hospital setting. We suggest that microwave technology could result in a substantial increase of patients reaching a stroke diagnosis in time for introduction of thrombolytic treatment. The socioeconomic ramifications of such a development are obvious not only in the industrial world but also, and perhaps even more so, in the developing world.

ACKNOWLEDGMENT

The authors acknowledge the company Medfield Diagnostics AB for financing and supporting the clinical measurements. Patient measurements were performed by research nurses Lina Håkansson and Leila Farashbandi, supported by engineer Stefan Kidborg.

REFERENCES

- [1] J. Olesen, A. Gustavsson, M. Svensson, H.U. Wittchen, B. Jönsson, "CDBE2010 study group; European Brain Council. The economic cost of brain disorders in Europe," *Eur J Neurol*. vol. 19, pp. 155–162, 2012.
- [2] The Atlas of Heart Disease and Stroke. *World Health Organization*, 2004.
- [3] T. Kjellström, B. Norrving, A. Shatchkute, "Helsingborg Declaration 2006 on European stroke strategies," *Cerebrovasc Dis*. vol. 23, pp. 231–241, 2007.
- [4] The National Institute of Neurological Disorders and Stroke rt-PA Stroke Study Group, "Tissue plasminogen activator for acute ischemic stroke," *N Engl J Med*. vol. 333, pp. 1581–1588, 1995.
- [5] H.P. Jr. Adams, G. del Zoppo, M.J. Alberts, et al. "Guidelines for the early management of adults with ischemic stroke: a guideline from the American Heart Association/American Stroke Association Stroke Council, Clinical Cardiology Council, Cardiovascular Radiology and Intervention Council, and the Atherosclerotic Peripheral Vascular Disease and Quality of Care Outcomes in Research Interdisciplinary Working Groups: The American Academy of Neurology affirms the value of this guideline as an educational tool for neurologists," *Circulation*, vol. 115, pp. e478–534, 2007.
- [6] European Stroke Organisation Executive Committee, "Guidelines for management of ischaemic stroke and transient ischaemic attack," *Cerebrovasc Dis*. vol. 25, pp. 457–507, 2008.
- [7] J.C. Grotta, W.S. Burgin, A. El-Mitwalli, M. Long, M. Campbell, L.B. Morgenstern, et al., "Intravenous tissue-type plasminogen activator therapy for ischemic stroke: Houston experience 1996 to 2000," *textitArch Neurol*, vol. 58, pp. 200–203, 2001.
- [8] A. Meretoja, D. Strbian, S. Mustanoja, T. Tatlisumak, P.J. Lindsberg, M. Kaste, "Reducing in-hospital delay to 20 minutes in stroke thrombolysis," *textitNeurology*, vol. 79, pp. 306–313, 2012.
- [9] K. Fassbender C. Balucani, S. Walter, S.R. Levine, A. Haass, J. Grotta, "Streamlining of prehospital stroke management: the golden hour," *textitLancet Neurology*, vol. 12, pp. 585–596, 2013.
- [10] G.W. Albers, J.M. Olivot, "Intravenous alteplase for ischaemic stroke," *Lancet*, vol. 369, pp. 249–250, 2007.
- [11] California Acute Stroke Pilot Registry (CASPR) Investigators. Prioritizing interventions to improve rates of thrombolysis for ischemic stroke. *Neurology* vol. 64, pp. 654–659, 2005.
- [12] S. Walter, P. Kostopoulos, A. Haass, et al, "Diagnosis and treatment of patients with stroke in a mobile stroke unit versus in hospital: a randomised controlled trial," *Lancet Neurol* vol. 11, pp. 397–404, 2012.
- [13] F. Schlachetzki, M. Herzberg, T. Hlscher, M. Ertl, M. Zimmermann, K.P. Ittner, et al. "Transcranial ultrasound from diagnosis to early stroke treatment: part 2: prehospital neurosonography in patients with acute stroke: the Regensburg stroke mobile project," *Cerebrovasc Dis*, vol. 33, pp. 262271, 2012.
- [14] C.H. Xu, L. Wang, X.T. Shi, F.S. You, F. Fu, R.G. Liu, et al. "Real-time imaging and detection of intracranial haemorrhage by electrical impedance tomography in a piglet model," *J Int Med Res*, vol. 38, pp.15961604, 2010.
- [15] G. Bonmassar, S. Iwaki, G. Goldmakher, L.M. Angelone, J.W. Belliveau, M.H.Lev, "On the measurement of electrical impedance spectroscopy (EIS) of the human head," *Int J Bioelectromagn*, vol. 12, pp. 3246, 2012.
- [16] S. Watanabe, N. Pakvasa, "Subspace methods in pattern recognition," *Proceedings of the 1st International Conference on Pattern Recognition*, pp. 25–32, 1973.
- [17] P. M. Meaney, M. W. Fanning, T. Raynolds, C. J. Fox, Q. Fang, C. A. Kogel S. P. Poplack, and K. D. Paulsen, "Initial Clinical Experience with Microwave Breast Imaging in Women with Normal Mammography," *Academic Radiology*, vol. 14, no. 2, pp. 207–218, Feb. 2007.
- [18] S. P. Poplack, T. D. Tosteson, W. A. Wells, B. W. Pogue, P. M. Meaney, A. Hartov, C. A. Kogel, S. K. Soho, J. J. Gibson, and K. D. Paulsen, "Electromagnetic Breast Imaging: Results of a Pilot Study in Women with Abnormal Mammograms," *Radiology*, vol. 243, no. 2. pp. 350–359, May 2007.
- [19] M. Klemm, I. Craddock, J. Leendertz, A. Preece, and R. Benjamin, "Experimental and clinical results of breast cancer detection using UWB microwave radar," in *2008 IEEE Antennas and Propagation Society International Symposium*, vol. 1–9, pp. 3014–3017, 2008.
- [20] K. R. Foster, J. L. Schepps, R. D. Stoy and H. P. Schwan, "Dielectric properties of brain tissue between 0.01 and 10 GHz," *Phys. Med. Biol*. vol. 24 pp. 1177–1187, 1979.
- [21] A. Peyman, S. J. Holden, S. Watts, R. Perrott, and C. Gabriel, "Dielectric properties of porcine cerebrospinal tissues at microwave frequencies: in vivo, in vitro and systematic variation with age," *Physics in Medicine and Biology*, vol. 52, no. 8, pp. 2229–2245, 2007.
- [22] S. Gabriel, R. W. Lau, and C. Gabriel, "The dielectric properties of biological tissues: II. Measurements in the frequency range 10 Hz to 20 GHz," *Physics in Medicine and Biology*, vol. 41, no. 11, pp. 2251–2269, 1996.
- [23] G. Schmid, G. Neubauer, and P. R. Mazal, "Dielectric properties of human brain tissue measured less than 10 h postmortem at frequencies from 800 to 2450 MHz," *Bioelectromagnetics*, vol. 24, no. 6, pp. 423–430, 2003.
- [24] A. Fhager, P. Hashemzadeh and M. Persson, "Reconstruction quality and spectral content of an electromagnetic time-domain inversion algorithm," *IEEE Trans Biomed. Eng.*, vol. 53, no. 8, pp. 1594–1604, Aug. 2006.
- [25] H. Dobšiček Trefná, M. Persson, "Antenna array design for brain monitoring," in *Proc. IEEE Antennas and Propagation Society International Symposium*, 2008, pp. 1–4.
- [26] M. A. Khorshidi, T. McKelvey, M. Persson and H. Dobšiček Trefná, "Classification of Microwave Scattering Data based on a Subspace Distance with Application to Detection of Bleeding Stroke," in *Proc. 3rd IEEE International Workshop on Computational Advances in Multi-Sensor Adaptive Processing (CAMSAP)*, pp. 301–304, Dec. 2009.
- [27] R. Scapatucci, O. M. Bucci, I. Catapano, and L. Crocco, "Differential Microwave Imaging for Brain Stroke Followup," *Int. Journal of Antennas and Propagation*, vol. 2014, Article ID 312528, 2014.
- [28] M. Guardiola, L. Jofre, S. Capdevila, J. Romeu, "UWB brain differential imaging capabilities," *6th European Conference on Antennas and Propagation (EUCAP)*, Gothenburh, Sweden, 26–30 March, 2012.
- [29] B.J. Mohammed, A.M. Abbosh, S. Mustafa, D. Ireland, "Microwave system for head imaging," *IEEE Trans Instrumentation and Measurement*, vol. 63, pp. 117–123, Jan., 2014.
- [30] A. Surowiec, S. S. Stuchly, A. Swarup, "Postmortem changes of the dielectric properties of bovine brain tissues at low radiofrequencies," *Bioelectromagnetics*, vol. 7, pp. 31–43, 1986.

- [31] H. Dobšiček Trefná, J. Vrba, M. Persson, "Evaluation of a patch antenna applicator for time reversal hyperthermia," *Int. J. Hyperthermia*, vol. 26, pp 185–197, March, 2010.
- [32] M.J. Ackerman, The Visible Human Project. *Journal of Biocommun*, vol. 18, pp. 14 ,1991.
- [33] M. A. Khorshidi, T. McKelvey, M. Persson, H. Dobšiček Trefná, "Classification of Microwave Scattering Data based on a Subspace Distance with Application to Detection of Bleeding Stroke," *The Third International Workshop on Computational Advances in Multi-Sensor Adaptive Processing*, Aruba, Dutch Antilles, Dec 13-16, 2009. ‘
- [34] L. Scharf, B. Friedlander, "Matched subspace detectors," *IEEE Trans. on Signal Processing*, vol. 42, pp. 2146–2157, 1994.
- [35] Y. Yu, T. McKelvey, " unified subspace classification framework developed for diagnostic system using microwave signal," *In Proc. of 21st European Signal Processing Conference (EUSIPCO)*, Marrakech, Marocco, Sept. 2013.
- [36] Yu Y. *Classification of High Dimensional Signals with Small Training Sample Size with Applications towards Microwave Based Detection Systems*, Lic. Thesis, Göteborg: Chalmers University of Technology. 2013.
- [37] T. Hastie, R. Tibshirani, and J. Friedman. *The Elements of Statistical Learning: Data Mining, Inference, and Prediction*. Springer, 2nd edition, 2009.
- [38] G. H. Golub and C. F. Van Loan, *Matrix Computations*, The Johns Hopkins University Press, Baltimore, Maryland, second edition, 1989.
- [39] B. Efron and R.J. Tibshirani. *An Introduction to the Bootstrap*, Chapman & Hall/CRC, 1994.
- [40] M.H. Zweig, G. Campbell, 'Receiver-operating characteristic (ROC) plots: a fundamental tool in clinical medicine,' *Clinical Chemistry* vol. 39, pp. 561–577, 1993.
- [41] A. Berglund A, L. Svensson, 'Higher prehospital priority level of stroke improves thrombolysis frequency and time to stroke unit: the Hyper Acute STroke Alarm (HASTA) Study,' *Stroke*, vol. 43, pp. 26662670, 2012.

APPENDIX A
PATIENT AND STROKE CHARACTERISTICS, CLINICAL STUDY 1

Table I

PATIENT AND STROKE CHARACTERISTICS, CLINICAL STUDY 1. ABBREVIATIONS: NIHSS NATIONAL INSTITUTES OF HEALTH STROKE SCALE, IS - ISCHEMIC STROKE, ICH - INTRACEREBRAL HAEMORRHAGE, F - FRONTAL, T - TEMPORAL, O - OCCIPITAL, P - PARIETAL, BG - BASAL GANGLIA, INS - INSULA, THAL - THALAMUS.

Age	Gender	Diagnosis	Site of lesion	Volume (ml)	Latency stroke to study (h:min)	NIHSS at investigation
39	F	IS	Right F	137	132:00	22
73	F	ICH	Left F	19	25:00	9
56	F	IS	Left T	16	55:05	14
68	M	IS	Right TO	29	77:10	5
59	M	IS	Left F	25	49:55	10
55	M	IS	Left FTP	287	128:00	14
64	F	ICH	Left BG	10	60:40	5
65	M	ICH	Left TP	19	19:38	7
65	M	IS	Right FTP	99	62:13	14
79	F	ICH	Right BG	3,3	26:10	7
64	F	IS	Right BG	6,0	94:20	4
76	M	IS	Left F, INS	22	47:10	11
46	F	IS	Left FTP	139	37:15	8
62	M	ICH	Right BG	6,8	36:10	4
86	M	ICH	Left BG	3,2	7:30	4
62	M	ICH	Left BG	17	23:35	18
70	F	ICH	Right THAL	4,0	21:15	5
53	M	ICH	Left THAL	0,5	19:40	2
37	M	IS	Right TF	53	26:05	1
64	F	IS	Left TO	47	27:55	13

APPENDIX B
PATIENT AND STROKE CHARACTERISTICS, CLINICAL STUDY 2

Table II

ABBREVIATIONS: NIHSS - NATIONAL INSTITUTES OF HEALTH STROKE SCALE, IS - ISCHEMIC STROKE, ICH INTRACEREBRAL HAEMORRHAGE, F - FRONTAL, T - TEMPORAL, O - OCCIPITAL, P - PARIETAL, BG - BASAL GANGLIA, INS - INSULA, THAL - THALAMUS, CAPS E - CAPSULA EXTERNA, COR RAD - CORONA RADIATA, VENT PEN VENTRICULAR PENETRATION, SAH PEN - SUBARACHNOIDAL HAEMORRHAGE PENETRATION, C SEMI CENTRUM SEMIOVALE, SDH - SUBDURAL HAEMORRHAGE.

Age	Gender	Diagnosis	Site of lesion	Volume (ml)	Latency stroke to study (h:min)	NIHSS at investigation
58	F	IS	Left FT, INS	36	18:10	2
73	F	IS	Right P	6,1	15:30	2
84	F	IS	Left CAPS E, INS	3,8	16:15	1
83	F	ICH	Left BG, VENT PEN	3,6	16:35	12
79	F	IS	Right COR RAD	0,7	10:30	2
68	M	ICH	Left FP, SAH PEN	13	26:45	13
89	F	ICH	Left C SEMI	2,5	21:30	22
40	M	ICH	Left BG	18	24:20	12
85	F	IS	Right T, INS	19	23:35	1
76	M	IS	Right F, BG	105	14:30	18
86	F	IS	Right F	2,2	25:05	6
60	M	IS	Right COR RAD	1,1	15:00	1
74	M	IS	Not visualized	-	20:55	0
53	F	ICH	Left THAL, VENT PEN	17	10:42	17
59	M	ICH	Left BG	2,4	4:28	4
65	F	IS	Right TP	48	21:52	1
83	F	IS	Left F	12	21:02	3
86	M	IS	Not visualized	-	4:57	9
62	M	IS	Right COR RAD	3,2	24:55	8
80	F	ICH	Right FP, SDH	18	13:16	10
89	F	IS	Left FT	206	19:27	26
82	F	IS	Right TP	38	6:27	17
61	F	ICH	Left BG, VENT PEN	35	20:05	22
89	F	ICH	Right BG, VENT PEN	82	23:44	11
67	F	ICH	Left THAL	3,1	11:28	7



Mikael Persson received his MSc and PhD degree from Chalmers University of Technology, Göteborg, Sweden, in 1982 and 1987, respectively. In 2000 he became professor in Electromagnetics and in 2006 Professor in Biomedical Electromagnetics at the Department of Signal and Systems, in Chalmers University of Technology. Since 2010 he is the head of the Division of Signal Processing and Biomedical engineering at Chalmers. His main research interests include electromagnetic diagnostics, monitoring and treatment, including microwave hyperthermia, stroke diagnostics, EEG source localization and microwave system design. He is author/co-author of more than 200 refereed journal and conference papers.



Tomas McKelvey received his Electrical Engineering education in Lund University between 1987 to 1991 and his PhD in Automatic Control at Linköping University in 1995. Between 1995 and 1999 he held research and teaching positions at Linköping University and became docent in 1999. Between 1999 and 2000 he was a visiting researcher at University of Newcastle, Australia. From 2000 he has been with Chalmers University of Technology, from 2006 he holds a full professor position and from 2011 he is the head of the Signal Processing group at Chalmers. Professor McKelvey's research interests are model based and statistical signal processing, system identification, control, machine learning and image processing with applications to biomedical engineering, active safety systems and combustion engines.



Andreas Fhager received the M.Sc. degree in engineering physics and the Ph.D. degree in electrical engineering from the Chalmers University of Technology, Göteborg, Sweden, in 2001 and 2006, respectively. He is currently Associate Professor and head of the Biomedical Electromagnetics research group at the department of Signals and Systems, Chalmers. His research interests are in signal processing, algorithm and systems development for microwave tomography and imaging intended for medical diagnosis and treatment applications.



Göran Pegenius received his BSc degree from the University of Göteborg, Sweden in 1986. Since 1995 he has had a position as research technician at the Dept of Clinical Neurophysiology, Sahlgrenska University Hospital and Sahlgrenska Academy in Gothenburg.



Hana Dobšiček Trefná received the M.Sc. degree in biomedical engineering from the Czech Technical University in Prague, Czech Republic and the Ph.D. degree in biomedical engineering from the Chalmers University of Technology, Göteborg, Sweden, in 2004 and 2010, respectively. She is currently Assistant Professor in the Biomedical Electromagnetics research group at the department of Signals and Systems, Chalmers. Her research interests include the engineering development and testing of microwave hyperthermia systems as well as other medical diagnosis and treatment applications of microwaves.



Jan-Erik Karlsson was born in Åmål, Sweden in 1960. He received the B.Sc. degree in Chemistry from the University of Göteborg, Sweden in 1989, and studied at the Medical School, Göteborg University 1981-1986. He received his PhD in Medicine at Göteborg University 1993. In 1994 he finished his internship at Mölndal County Hospital and received the MD licence. After residency at the Dept of Neurology, Sahlgrenska University Hospital, Göteborg, he was appointed Specialist in Neurology 2000. He was appointed Senior Consultant in Neurology and head of the Stroke Unit at Sahlgrenska University Hospital 2002 and has held this position since. His clinical research work has focused on acute stroke treatments, mainly intravenous thrombolysis and endovascular intervention treatments. He has participated as investigator and principal investigator in about 15 clinical trials, both academic and industrial.



Yinan Yu received her Bachelor of Science degree in communication engineering from Nankai University, Tianjin, China and the Master of Science degree in communication engineering from Chalmers University of Technology, Gothenburg, Sweden. She is currently pursuing a Ph.D. degree on the subject of signal reconstruction and classification at Chalmers University of Technology, Göteborg, Sweden. From March 2013 to March 2014, she was a visiting student at Princeton University, Princeton, USA. Her research interests are in the areas of machine learning techniques for multi-class, multi-label classification problems, feature transformation and selection for reducing complexity, kernel analysis and techniques of handling large-scale data.



Mikael Elam received his MD at the University of Göteborg in 1982 and specialist certification in Clinical Neurophysiology at the Sahlgrenska University Hospital in Göteborg in 1990, where he was appointed senior consultant in 1995. Academically, he received a PhD in experimental neurophysiology/neuropharmacology in 1985, became an associate professor in 1990 and professor/chairman of the Göteborg department of Clinical Neurophysiology in 2001. His main research focus is on autonomic neuroscience, including central and peripheral nervous system control of cardiovascular function. He has authored/co-authored more than 130 peer-reviewed original research publications; Hirsch index 32.